# Solitary and periodic waves in collisionless plasmas: The Adlam-Allen model revisited

J. E. Allen,[1] D. J. Frantzeskakis,[2] N. I. Karachalios,[3] P. G. Kevrekidis,[4,1] and V. Koukouloyannis[3]

[1]*Mathematical Institute, University of Oxford, Oxford OX2 6GG, United Kingdom*

[2]*Department of Physics, National and Kapodistrian University of Athens, Panepistimiopolis, Zografos, Athens 15784, Greece*

[3]*Department of Mathematics, Laboratory of Applied Mathematics and Mathematical Modelling, University of the Aegean, Karlovassi, 83200 Samos, Greece*

[4]*Department of Mathematics and Statistics, University of Massachusetts, Amherst, Massachusetts 01003-4515, USA*

(Received 13 February 2020; accepted 24 June 2020; published 20 July 2020)

We consider the Adlam-Allen (AA) system of partial differential equations, which, arguably, is the first model that was introduced to describe solitary waves in the context of propagation of hydrodynamic disturbances in collisionless plasmas. Here, we identify the solitary waves of the model by implementing a dynamical systems approach. The latter suggests that the model also possesses periodic wave solutions—which reduce to the solitary wave in the limiting case of an infinite period—as well as rational solutions that are obtained herein. In addition, employing a long-wave approximation via a relevant multiscale expansion method, we establish the asymptotic reduction of the AA system to the Korteweg–de Vries equation. Such a reduction is not only another justification for the above solitary wave dynamics, but may also offer additional insights for the emergence of other possible plasma waves. Direct numerical simulations are performed for the study of multiple solitary waves and their pairwise interactions. The stability of solitary waves is discussed in terms of potentially relevant criteria, while the robustness of spatially periodic wave solutions is touched upon via numerical experiments.

DOI: 10.1103/PhysRevE.102.013209

## I. INTRODUCTION

The fundamental work of Adlam and Allen in 1958 and 1960 [1,2] constituted one of the very first examples of models that may exhibit solitary-wave dynamics, arguably the very first one in the important field of plasma physics. Indeed, this work preceded the hallmark efforts of Kruskal and Zabusky in 1965 [3] concerning the study of solitary waves and their interactions in the context of the famous Fermi-Pasta-Ulam problem [4] and its connections with the Korteweg–de Vries (KdV) equation [5]. In addition, the Adlam-Allen (AA) model and its solitary wave was introduced earlier than the seminal work of Washimi and Taniuti [6], who showed that the one-dimensional (1D) long-time asymptotic behavior of small-amplitude ion-acoustic waves in plasmas is described by the KdV equation. The above works paved the way for numerous investigations in the nonlinear physics of plasmas, which proved to be a fertile ground for the study of solitary waves and solitons in integrable and nearly integrable equations [7,8]. In view of the above, the AA model seems to have received far less than its share of interest and associated research attention within the field of nonlinear waves and solitons, as has been discussed, e.g., in Ref. [9]. A recent revisiting of the relevant subject can be found in Ref. [10], where the role of the so-called $j \times B$ force in a collisionless plasma was discussed.

Our aim in the present work is to revisit the AA model. In particular, upon shortly introducing the original motivation and formulation of the AA system of partial differential equations (PDEs), we start from its reduced—and more tractable for analysis—form presented in Ref. [2]. First we derive the Lagrangian density of the system, as well as the Hamiltonian density and momentum of the system. Then, we study the linear regime and show that the AA model features the linear dispersion relation of the improved Boussinesq equation, which is known to describe bidirectional shallow water waves [11]. Proceeding further, we seek traveling waves that can be supported by the model, and use techniques from the theory of nonlinear dynamical systems to study the associated second-order ordinary differential equation (ODE). We identify exact and analytically expressed (as per the original efforts of [1,2]) solitary waves, corresponding to homoclinic orbits in the associated phase plane of the conservative dynamical system. We find that these waves have speeds between one and two times the characteristic Alfvén speed [1]. This dynamical systems approach also enables the identification of periodic orbits, reminiscent of the elliptic function solutions (corresponding to the so-called "cnoidal waves") of the KdV equation; these periodic orbits correspond to spatially periodic solutions of the original AA system. Interestingly, a degenerate case of the relevant ODE, corresponding to the case in which the traveling wave propagates with exactly the Alfvén speed, leads to the existence of a rational-type solution. Furthermore, by implementing a suitable multiscale asymptotic expansion, based on a long-wave approximation, we show that the original AA system can be approximated by the KdV equation, and that—in the small-amplitude limit—the exact solitary waves of the AA system reduce to the KdV solitons.

The above strong justification for the potential of solitary-wave dynamics motivates us to study the interaction of multiple solitary waves of the AA model by direct numerical simulations. When colliding two such waves, we find the interaction between them to be nearly (but not completely) elastic with a clearly observable phase shift between the two

 

solitary waves. While our findings suggest that the AA model is likely not to be completely integrable, further investigation of the relevant topic is certainly worthwhile. We also perform a numerical study on perturbations of the identified spatially periodic solutions, which suggests their potential robustness. Furthermore, we show that in the small-amplitude (KdV) limit, the stability of the traveling waves is justified by the relevant stability criterion (of a Vakhitov-Kolokolov type [12], namely involving the derivative of a conserved quantity such as the momentum with respect to the corresponding Lagrange multiplier, namely the speed, described herein) for KdV-type equations; see, e.g., [13–16] as well as references therein. Interestingly, the monotonicity (implying stability) of the relevant momentum dependence on speed is preserved throughout the interval of speeds for which the AA solitary waves are physically relevant, being suggestive of a qualitatively similar result for arbitrary speeds; nevertheless, admittedly we can only support this on the basis of the above criterion for speeds near the Alfvén speed. In an interesting parallel development, we leverage recent work on quadratic operator pencils [17] to illustrate that an analogous criterion for Klein-Gordon-type equations also exists on the basis of the Klein-Gordon momentum and its monotonic dependence on the speed. We have also evaluated the relevant quantity and have shown that the corresponding sign of the derivative is also one that reflects stability in the Klein-Gordon case. While the present model is neither of the KdV nor of the Klein-Gordon type, the fulfillment of these stability criteria, together with the results of direct numerical simulations, allows us to conjecture the generic stability of the AA model traveling waves. Finally, we comment on the case of rational solutions due to their mathematical interest.

Here, we should make a few remarks regarding the applicability of our results in plasma physics. First, we should point out that, although we establish a strong connection of the AA model with the KdV equation, which is known to describe nonlinear ion-acoustic waves in plasmas (see, e.g., Ref. [7]), the waves supported by the AA model are not directly related to ion-acoustic waves. Indeed, the AA model describes "hydrodynamic waves" in quasineutral collisionless plasmas propagating perpendicular to a magnetic field. In comparison, e.g., with the classic work of [6] on ion-acoustic waves, our model bears velocity both along the $x$- and the $y$-direction (although both are $x$-dependent) and features both magnetic, as well as electric fields, as opposed to the single-speed and solely electric-field dependence of [6]. Second, regarding the applicability of the AA model, first we note that the early work [1] was carried out in the early days of fusion research. Thus, the waves supported by the AA model—which is the main theme of this work—may find applications in fusion research, but also in astrophysical observations. In astrophysics, such waves may be associated with the Earth's bow shock [18], coronal mass ejections [19], and plasma release experiments [20]. More practically, at a physical level, the AA model describes the waves associated with the evolution of charged particles (ions and electrons under quasineutrality conditions) emerging when assuming planar propagation of the particles with all quantities assumed to depend only along the traveling direction $x$ and the magnetic field is transverse to the direction of motion. Remarkably this situation appears to feature solitary-wave propagation due to the effective nonlinearity of the $j \times B$ force [10], but also, as shown below, to enable periodic traveling waves to arise.

The presentation of the paper is as follows: In Sec. II, we describe the AA model, and we present our analytical approaches for the identification of the exact solitary-wave solutions and the connection of the model to the KdV equation. In Sec. III, we present the results of our numerical studies. Section IV summarizes our findings and briefly discusses potential future studies for the AA and other related models.

## II. THE MODEL AND ITS ANALYTICAL CONSIDERATION

### A. Presentation of the AA model

The study of Refs. [1,2] concerned electrons and ions in a plasma, where the magnetic field is in the $z$-direction, and no variations of the pertinent fields along the $y$ or $z$ directions were considered. Furthermore, it was assumed that appreciable amounts of energy are given to the particles in the waves (e.g., 10 keV—see Ref. [1]). The applications of that work were intended to lie both in the field of fusion research as well as in the study of astrophysical phenomena, such as the solar wind [21].

Let us denote by $U_1, U_2$ the velocities along the $x$-direction of two distinct masses $m_1$ and $m_2$ and the corresponding velocities along the $y$-direction by $V_1$ and $V_2$. We express the densities as $n_1, n_2$ and the charges as $e_1, e_2$, with $e_1 + e_2 = 0$. Then, the force balance equations and Maxwell field equations are

$$U_{1,t} + U_1 U_{1,x} = \frac{e_1}{m_1}\left[E_x + \frac{V_1 B_z}{c}\right], \tag{1}$$

$$V_{1,t} + U_1 V_{1,x} = \frac{e_1}{m_1}\left[E_y - \frac{U_1 B_z}{c}\right], \tag{2}$$

$$U_{2,t} + U_2 U_{2,x} = \frac{e_2}{m_2}\left[E_x + \frac{V_2 B_z}{c}\right], \tag{3}$$

$$V_{2,t} + U_2 V_{2,x} = \frac{e_2}{m_2}\left[E_y - \frac{U_2 B_z}{c}\right], \tag{4}$$

$$\frac{\partial H_z}{\partial x} = -\frac{4\pi}{c}[n_1 e_1 V_1 + n_2 e_2 V_2], \tag{5}$$

$$\frac{\partial E_y}{\partial x} = -\frac{1}{c}\frac{\partial B_z}{\partial t}, \tag{6}$$

where $c$ denotes the speed of light. It is now assumed that the velocities along the $x$-direction are equal, i.e., $U_1 = U_2$, and similarly the densities for the electrons and ions are also equal, i.e., $n_1 = n_2$; thus, the relative velocity between them can be referred to as $V = V_1 - V_2$. A key consideration here is the *quasineutrality* of the plasma. This means that there is a very small difference between $n_1$ and $n_2$ responsible for the electric field, yet we may approximately assume $n_1 = n_2 \equiv n$ for practical purposes, an assumption that is valid when the electron plasma frequency is much greater than the electron gyrofrequency. The relevant criterion given in Ref. [1] also provides the condition for the nonrelativistic equations to be valid.

One can then switch to a Lagrangian (moving with the particles) coordinate system and adimensionalize over characteristic scales of the magnetic field $B_\star$ (i.e., $B \mapsto B/B_\star$)

and density $n_\star$ (i.e., $n \mapsto n/n_\star$). In this framework, the speed is measured in units of the characteristic Alfvén speed, $V_A = \sqrt{B_\star^2/[4\pi\mu n_\star(m_1+m_2)]}$, where $\mu$ stands for the magnetic permeability of free space, while the electric field is measured in units of $E_\star = V_A B_\star/c$, i.e., $E \mapsto E/E_\star$. Finally, the space variables $(x, y, z)$ are measured in units of $d = \sqrt{m_1 m_2 c^2/[4\pi n_\star \mu e_2^2(m_1+m_2)]}$, while time is measured in units of $t_\star = (m_1 m_2)^{1/2} c/(e_2 B_\star)$, i.e., $t \mapsto t/t_\star$. As a result, we obtain the dimensionless Adlam-Allen (AA) model, described by the following system of PDEs:

$$R_{tt} = -\tfrac{1}{2}(B^2)_{xx}, \tag{7}$$

$$B_{txx} = (RB)_t. \tag{8}$$

Here, $B$ is the rescaled (by $B_\star$) magnetic field, while $R = n_\star/n_{1,2}$ is the rescaled (inverse) density of ions and electrons. Our intention hereafter is to work with this reduced dimensionless version of the AA model.

### B. Fundamental properties of the AA model

#### 1. The AA system with vanishing boundary conditions

The simplest nontrivial solution of the AA model (7) and (8) is expressed in the form

$$R = R_0, \quad B = B_0, \tag{9}$$

where the constants $R_0$ and $B_0$ set the boundary conditions (BCs) at infinity, namely $R \to R_0$ and $B \to B_0$ as $x \to \pm\infty$. Integrating Eq. (8) over time, and using the aforementioned BCs, we can express the AA model as

$$R_{tt} = -\tfrac{1}{2}(B^2)_{xx}, \tag{10}$$

$$B_{xx} = RB - R_0 B_0. \tag{11}$$

It is now convenient to seek solutions of the AA model on top of the background solution, $R = R_0$ and $B = B_0$, namely

$$R(x,t) = R_0 + u(x,t), \quad B(x,t) = B_0 + w(x,t), \tag{12}$$

with the unknown fields $u$ and $w$ satisfying vanishing BCs at infinity, namely $u, w \to 0$ as $x \to \pm\infty$. Substituting Eq. (12) into Eqs. (10) and (11), we obtain the following system of nonlinear PDEs for the fields $u$ and $w$:

$$u_{tt} + B_0 w_{xx} + \tfrac{1}{2}(w^2)_{xx} = 0, \tag{13}$$

$$w_{xx} - R_0 w - B_0 u - uw = 0. \tag{14}$$

#### 2. Lagrangian structure and integrals of motion

It can now be shown that the system of Eqs. (13) and (14) can be derived by the Euler-Lagrange equations of fields described by a certain Lagrangian density. To derive a Lagrangian for the above system, we follow the methodology used in Ref. [22] for the derivation of the Lagrangian of the Zakharov equations (see, e.g., Ref. [7]), We thus introduce the auxiliary field $\rho(x,t)$, such that

$$u \equiv \rho_x. \tag{15}$$

Inserting Eq. (15) in Eqs. (13) and (14), and integrating (13) once with respect to $x$, the AA system is cast in the form

$$\rho_{tt} + B_0 w_x + \tfrac{1}{2}(w^2)_x = 0, \tag{16}$$

$$w_{xx} - R_0 w - B_0 \rho_x - \rho_x w = 0. \tag{17}$$

Then, it can be found that Lagrangian density corresponding to Eqs. (16) and (17) is of the form

$$\mathcal{L} = \tfrac{1}{2}\rho_t^2 + \tfrac{1}{2}w_x^2 + \tfrac{1}{2}R_0 w^2 + \tfrac{1}{2}\rho_x w^2 + B_0 \rho_x w,$$

with the full Lagrangian $L$ defined as the integral of the Lagrangian density, namely $L = \int_{-\infty}^{+\infty} \mathcal{L} dx$. Indeed, it is straightforward to check that the Euler-Lagrange equations:

$$\frac{\partial}{\partial t}\left(\frac{\partial \mathcal{L}}{\partial \Phi_{i,t}}\right) + \frac{\partial}{\partial x}\left(\frac{\partial \mathcal{L}}{\partial \Phi_{i,x}}\right) - \frac{\partial \mathcal{L}}{\partial \Phi_i} = 0,$$

where $\Phi_i$ (with $i = 1, 2$) is a generic name for the fields $\rho(x,t)$ and $w(x,t)$, respectively, lead to Eqs. (16) and (17). Furthermore, we can define momentum densities $\pi_i = \partial\mathcal{L}/\partial\Phi_{i,t}$, and also introduce the Hamiltonian density $\mathcal{H}$, through the Legendre transformation $\mathcal{H} = \sum_i \pi_i \Phi_{i,t} - \mathcal{L}$. Observing that $\pi_1 = \rho_t$ and $\pi_2 = 0$, we find that $\mathcal{H} = \rho_t^2 - \mathcal{L}$. Hence, the system possesses an important conserved quantity, namely the total energy (full Hamiltonian), given by

$$H \equiv \int_{-\infty}^{+\infty} \mathcal{H}\, dx = \int_{-\infty}^{+\infty} \left(\frac{1}{2}\rho_t^2 - \frac{1}{2}w_x^2 - \frac{1}{2}R_0 w^2 - \frac{1}{2}\rho_x w^2 - B_0 \rho_x w\right) dx.$$

On the other hand, the system (13) and (14) possesses another important conserved quantity, namely the momentum, which is given by

$$P \equiv \int_{-\infty}^{+\infty} \mathcal{P}\, dx = -\int_{-\infty}^{+\infty} \rho_t \rho_x dx.$$

Indeed, $dP/dt = \int_{-\infty}^{+\infty}(\rho_{tt}\rho_x + \rho_t \rho_{xt})dx = \int_{-\infty}^{+\infty} w_x(R_0 w - w_{xx}) + \frac{1}{2}(\rho_t^2)_x dx = 0$, due to the fact that $w$ and $\rho_t$ are assumed to satisfy vanishing BCs at infinity. Note that, in the case of traveling-wave solutions that we study below, i.e., for $u = u(\xi)$ with $\xi = x - vt$, it is straightforward to find that the momentum $P$ is reduced to the form

$$P = v \int_{-\infty}^{+\infty} u^2 dx. \tag{19}$$

#### 3. The linear regime and connection with the Boussinesq equation

Let us now consider elementary solutions of the AA model, in the form of linear waves, close to the background solution (9). To find such solutions, we assume that $u, w \sim O(\epsilon)$, where $0 < \epsilon \ll 1$ is a small parameter. Then, at order $O(\epsilon)$, the linearization of Eqs. (13) and (14) leads to the following linear equations:

$$u_{tt} + B_0 w_{xx} = 0, \tag{19}$$

$$w_{xx} - R_0 w - B_0 u = 0. \tag{20}$$

Obviously, using Eq. (20), one may substitute $u = (w_{xx} - R_0 w)/B_0$ into Eq. (19) and arrive at the following equation

for $w$:

$$w_{tt} - C^2 w_{xx} - \frac{1}{R_0} w_{xxtt} = 0, \tag{21}$$

where

$$C^2 \equiv \frac{B_0^2}{R_0} \tag{22}$$

is the square of the speed of small-amplitude linear waves in the long-wavelength (small $k$) limit; see also Eq. (23) below. Equation (21) has the form of a linearized *improved* Boussinesq equation (iBE) [23]. Generally, the Boussinesq model is known to describe the evolution of bidirectional shallow water waves [11], and the dynamics of pulses in nonlinear lattices (through a continuous approximation) [24]. A crucial difference between the standard Boussinesq equation and its iBE variant is that the latter is not prone to unphysical long-wavelength instabilities (see, e.g., Ref. [25]). The linearized iBE (21) admits plane-wave solutions, $\sim \exp[i(kx - \omega t)]$, with the frequency $\omega$ and wave number $k$ obeying the dispersion relation:

$$\omega^2 = C^2 k^2 \left(1 + \frac{k^2}{R_0}\right)^{-1}. \tag{23}$$

Considering long waves and weak dispersion, such that $k^2/R_0 \ll 1$, and focusing on the case of right-going waves, we may approximate the dispersion relation (23) as $\omega \approx Ck - (C/2R_0)k^3$, which is the dispersion relation of a Korteweg–de Vries (KdV) equation. This indicates a strong connection of the AA model with the KdV equation. Indeed, below we will show that the AA model possesses exact traveling-wave solutions in the form of solitary waves, which—in the small-amplitude limit—transform into the KdV solitons.

### C. Derivation of exact traveling waves

Let us now proceed by seeking solutions of the system (13) and (14) in the form of traveling waves, namely

$$u = u(\xi), \quad w = w(\xi); \quad \xi \equiv x - vt, \tag{24}$$

where $v$ denotes the velocity of the waves. Recalling that $u, w \to 0$ as $x \to \pm\infty$, Eq. (13) can readily be integrated twice with respect to $\xi$, leading to

$$u = -\frac{1}{v^2}\left(B_0 w + \frac{1}{2} w^2\right). \tag{25}$$

Substituting Eq. (25) into Eq. (14), we obtain the following nonlinear ODE for the field $w$:

$$w'' = \frac{B_0^2}{v^2 C^2}(v^2 - C^2) w - \frac{3B_0}{2v^2} w^2 - \frac{1}{2v^2} w^3, \tag{26}$$

where the primes denote differentiation with respect to $\xi$. Equation (26) can be viewed as an equation of motion of a particle in the presence of the effective potential $V(w)$ given by

$$V(w) = -\frac{B_0^2}{2v^2 C^2}(v^2 - C^2) w^2 + \frac{B_0}{2v^2} w^3 + \frac{1}{8v^2} w^4. \tag{27}$$

The total energy of this dynamical system is

$$E(w, w') = \tfrac{1}{2} w'^2 + V(w) = E_0, \tag{28}$$

where the constant of integration $E_0$ represents the total initial energy of the effective oscillator, which is conserved along its motion.

A simple analysis shows that if $v < C$, then there exists a sole fixed point at $w = 0$ being a stable center, at which the potential $V$ attains its global minimum. As a result, all solutions of Eq. (26) are periodic and can, in principle, be expressed in terms of the Jacobi elliptic functions [26].

On the other hand, if $v > C$ there exist for $w \geqslant 0$ two fixed points: an unstable saddle point at $w = 0$ (corresponding to the global maximum of the potential $V$ for $w \geqslant 0$) and a stable center at $w = 8(v/C - 1)B_0$ (corresponding to the global minimum of $V$ for $w \geqslant 0$). The graph of the potential $V(w)$ (27) in this case is portrayed in Fig. 1(a). This is a case of particular interest, since there exists a homoclinic orbit (separatrix), namely a trajectory of infinite period, which corresponds to a solution decaying at infinity, i.e., a solitary wave. Figure 1(b) depicts orbits of the dynamical system (26) corresponding to various energy values [straight horizontal lines shown in the graph of the potential $V(w)$, depicted in panel (a)]. The homoclinic orbit [continuous (red) curve forming a "loop" as shown in panel (b)] corresponds to the energy $E_0 = V(0) = 0$ [see the continuous (red) horizontal line shown in panel (b)]. The closed orbits [dashed (blue) curves] correspond to energy values $E_0 < 0$, and they are associated with spatially periodic solutions. These solutions will be discussed in Sec. III D.

Let us focus on the homoclinic orbit. To derive the corresponding solution, we use the first integral [see Eq. (28)] for the value $E_0 = 0$, which is the energy of the homoclinic solution. Then, a second integration, i.e., $\int dw/\sqrt{-2V(w)} = \xi - x_0$ ($x_0$ is an integration constant), leads to the implicit form of the solution, which eventually can be expressed in the following explicit form:

$$w(x,t) = \frac{2B_0}{C}(v^2 - C^2)\frac{1}{C + v\cosh(\theta)}, \tag{29}$$

$$\theta \equiv \frac{B_0}{vC}\sqrt{v^2 - C^2}(x - vt - x_0). \tag{30}$$

In Eq. (30), the integration constant $x_0$ represents the initial position of the solitary wave. Notice that due to the aforementioned necessary condition, $v > C$, for the existence of the solitary wave (29), it turns out that this exact traveling-wave solution is in fact traveling with a speed larger than that of the long-wavelength linear waves. On the other hand, the constraint for a positive density, $R > 0$, yields [using Eqs. (12), (25), and (29)] an upper bound for the speed, namely $v < 2C$. Thus, in terms of the velocity $v$, the domain of existence of a physically relevant solitary wave is

$$C < v < 2C. \tag{31}$$

Summarizing our findings presented in this section, we have derived an exact, exponentially localized, traveling-wave solution of the AA model of the form

$$R(x,t) = R_0 - \frac{1}{v^2} w(x,t)\left[B_0 + \frac{1}{2} w(x,t)\right] := R^s(x,t), \tag{32}$$

$$B(x,t) = B_0 + w(x,t) := B^s(x,t), \tag{33}$$

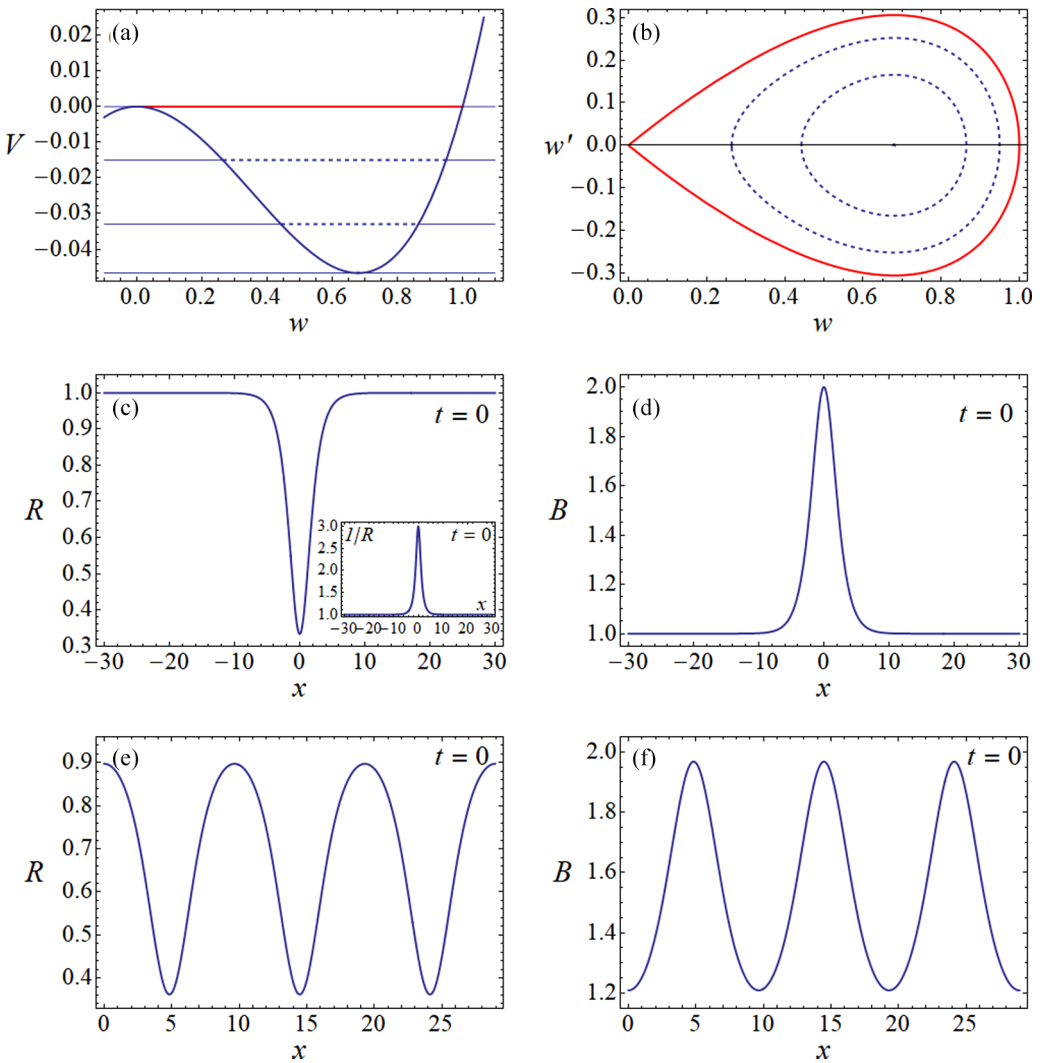


FIG. 1. Top row: Panel (a) shows the effective potential $V(w)$ (27), along with some typical energy levels depicted by straight horizontal lines. Parameter values: $B_0 = R_0 = 1$, $v = 1.5$. The continuous (red) line corresponds to the energy $E_0 = V(0) = 0$ corresponding to the homoclinic orbit. The dashed lines depict energy values $E_0 < 0$, which correspond to closed, periodic orbits. Panel (b) shows orbits in the $(w, w')$ phase-plane of Eq. (26), corresponding to the energy levels of panel (a). The continuous (red) curve depicts the homoclinic orbit, pertinent to the energy $E_0 = V(0) = 0$. The dashed closed curves are associated with the periodic solutions corresponding to energy values $E_0 < 0$. Middle row: Panel (c) shows the profile of the solitary wave for $R$, given by Eq. (32), at $t = 0$. Shown also, as an inset, is the quantity $1/R$, which, physically, represents the density of the charged particles. Panel (d) shows the profile of the soliton solution for $B$ given by (33), at $t = 0$. Bottom row: A spatially periodic solution corresponding to the energy $E_0 = -0.015$. Panel (e) depicts the profile of the $R^p$ periodic component of the solution, at $t = 0$, while panel (f) depicts the profile of its $B^p$ periodic component, at $t = 0$.

with $w(x, t)$ given by Eqs. (29) and (30). This is the same wave as was identified in Ref. [1], yet the approach used herein will enable us to obtain a considerably wider family of solutions in what follows. The profiles of these solutions at $t = 0$ are depicted in the middle row of Fig. 1. Figure 1(c) shows the profile of $R^s(x, 0)$, and Fig. 1(d) shows the profile of $B^s(x, 0)$ corresponding to a pulse on top of the finite background $B_0 = 1$. The inset of panel (c) also shows $1/R$, which is proportional to the particle density.

### D. Connection to the KdV equation

The derivation of the linearized iBE (21) that describes the linear properties of the model, as discussed in Sec. II B, suggests the possibility of establishing an asymptotic connection between the AA system and the KdV equation. To do this, it is convenient to employ the long-wave approximation [23]. In particular, taking into consideration that for long waves the dispersion relation (23) can be approximated as $\omega \approx Ck - (C/2R_0)k^3$, we may assume that the wave number $k$ is of the order $O(\epsilon^p)$, where $0 < \epsilon \ll 1$ is a formal small parameter, and $p > 0$. Notice that, as we will see, the choice of $p$ is not important; hence, without loss of generality, we choose $p = 1/2$. Then, the substitution $k \mapsto \epsilon^{1/2}k$ into the dispersion relation leads to the frequency $\omega \approx \epsilon^{1/2}Ck - \epsilon^{3/2}(Ck^3/2R_0)$. Accordingly, the phase of the plane-wave solution of the linearized iBE, Eq. (21), reads $kx - \omega(k)t \approx \epsilon^{1/2}k(x - Ct) + \epsilon^{3/2}(Ck^3/2R_0)t$. This suggests the introduction of the follow-

ing slow variables:

$$X = \epsilon^{1/2}(x - Ct), \quad T = \epsilon^{3/2}t. \tag{34}$$

Notice that this choice is consistent with the fact that, in the long-wavelength limit of $k \to 0$, the asymptotic behavior of the solution of the iBE is [23] $u(x,t) \sim \mathrm{Ai}(z)$, where $\mathrm{Ai}(z) \equiv (1/\pi)\int_0^{+\infty}\cos(sz + \frac{1}{3}s^3)ds$ is the Airy function, and $z = (x - Ct)/[(3C/2R_0)^{1/3}t^{1/3}]$. In other words, the asymptotic analysis suggests a similarity behavior for a coordinate system with $z = \text{const}$, which is obviously valid for the choice of the coordinate system of Eq. (34).

Using the above slow variables, Eqs. (13) and (14) are expressed, respectively, as follows:

$$\epsilon\left(C^2 - \frac{B_0^2}{R_0}\right)w_{XX} - \epsilon\frac{1}{R_0}\partial_X^2\left(\frac{1}{2}B_0w^2 - C^2uw\right) - \epsilon^2\left(2Cw_{XT} - \frac{C^2}{R_0}w_{XXXX}\right) = O(\epsilon^j), \quad j \geqslant 3, \tag{35}$$

$$\epsilon w_{XX} - R_0 w - B_0 u - uw = 0. \tag{36}$$

It can now readily be observed that the first term on the right-hand side of Eq. (35) vanishes—see Eq. (22). Furthermore, we introduce the following perturbation expansions of the fields $u$ and $w$ with respect to $\epsilon$:

$$u = \epsilon u_1 + \epsilon^2 u_2 + \cdots, \quad w = \epsilon w_1 + \epsilon^2 w_2 + \cdots, \tag{37}$$

where the powers in $\epsilon$ are chosen so that the dominant dispersion term and the dominant nonlinearity term are of the same order; this choice, as we will see, gives rise to soliton solutions. Substituting, we can obtain from Eqs. (35) and (36) the following results. First, at order $O(\epsilon)$ we derive from Eq. (36) the following equation connecting the unknown fields $u_1$ and $w_1$:

$$u_1 = -\frac{R_0}{B_0}w_1. \tag{38}$$

Next, using Eq. (38), the nonlinear contribution [second term in Eq. (36)] arising at $O(\epsilon^3)$ in Eq. (36) becomes $-(3B_0/R_0)(w_1w_{1X})_X$. As a result, at $O(\epsilon^3)$, integration of Eq. (36) over $X$ leads to the following KdV equation:

$$2Cw_{1T} + \frac{C^2}{R_0}w_{1XXX} + \frac{3B_0}{R_0}w_1w_{1X} = 0. \tag{39}$$

It is well known that the KdV equation is a completely integrable system possessing soliton solutions (see, e.g., Ref. [11]). In particular, the single soliton solution of Eq. (39), when expressed in terms of the original variables $x$ and $t$, gives rise to the following approximate solution [valid up to order $O(\epsilon)$] of the system (13) and (14):

$$w(x,t) = \epsilon\kappa^2\frac{4B_0}{R_0}\mathrm{sech}^2(\eta), \tag{40}$$

$$u(x,t) = -4\epsilon\kappa^2\mathrm{sech}^2(\eta), \tag{41}$$

$$\eta \equiv \epsilon^{1/2}\kappa\left[x - C\left(1 + \epsilon\kappa^2\frac{2}{R_0}\right)t - x_0\right], \tag{42}$$

where $\kappa$ is an arbitrary $O(1)$ parameter characterizing the amplitude, the width, and the velocity of the KdV soliton. Thus, the original AA system (7) and (8) supports the following approximate solution:

$$R(x,t) \approx R_0\left[1 - \epsilon\frac{4\kappa^2}{R_0}\mathrm{sech}^2(\eta)\right], \tag{43}$$

$$B(x,t) \approx B_0\left[1 + \epsilon\frac{4\kappa^2}{R_0}\mathrm{sech}^2(\eta)\right]. \tag{44}$$

We will now show that in the limit of $v \to C$, the solitary wave (29) becomes the KdV soliton (40). To do this we use $v \approx C$, and we approximate $v^2 - C^2$ as follows: $v^2 - C^2 = (v + C)(v - C) \approx 2C(v - C)$. Then, using the identity $1 + \cosh(\theta) = 2\cosh^2(\theta/2)$, we may rewrite Eq. (29) in the form

$$w(x,t) = \frac{2B_0}{C}(v - C)\mathrm{sech}^2\left[\frac{B_0}{2vC}\sqrt{v^2 - C^2}(x - vt - x_0)\right]. \tag{45}$$

It is now evident that much like the KdV soliton, the amplitude and width of the solitary wave (45) are set by a single parameter, namely $v - C$. The limit $v \to C$ is in fact equivalent to the small-amplitude limit, whereby $v - C$ plays now the role of a small parameter. Then, employing the small parameter $\epsilon$, and noticing that $\kappa^2(4B_0/R_0) = O(1)$ as per our analysis, we can set $v - C = \epsilon\kappa^2C(2/R_0)$. This automatically implies that the amplitudes of the solitary wave (45) and the KdV soliton (40) are equal. Furthermore, it can readily be observed that the velocity of the solitary wave (45) becomes

$$v = C[1 + \epsilon\kappa^2(2/R_0)],$$

which is equal to the velocity of the KdV soliton (40). Finally, the inverse width of the solitary wave (45) reads

$$\frac{B_0}{2vC}\sqrt{v^2 - C^2} \approx \frac{B_0}{2vC}\sqrt{2C(v - C)} = \frac{B_0}{2vC}\sqrt{2C^2\epsilon\kappa^2(2/R_0)} = \epsilon^{1/2}\kappa,$$

where we have used the definition of the velocity $C$ in Eq. (22). Thus, the inverse width of the solitary wave (45) becomes equal to that of the KdV soliton (40). Hence, we have shown that in the limit $v \to C$, i.e., in the small-amplitude limit, the solitary wave (45) transforms into the KdV soliton (40), which further highlights the asymptotic connection of the AA model with the KdV equation.

Concluding this section, it is also relevant to make some additional comments. The derivation of the KdV equation and the soliton solution relies on the leading-order solution [Eq. (38)] of Eq. (36), which is a singularly perturbed equation. In principle, this equation could support boundary-layer-type solutions; nevertheless, the derivation of such solutions demands a consistent treatment of the full system, i.e., both Eqs. (35) and (36). This would lead to higher-order corrections to the KdV equation and the soliton solution thereof. This is indeed a very interesting problem, but a relevant study is beyond the scope of this work.

### E. A rational solution

As was shown in Sec. II B, the AA system supports the exact, exponentially localized, solitary-wave solutions (32)

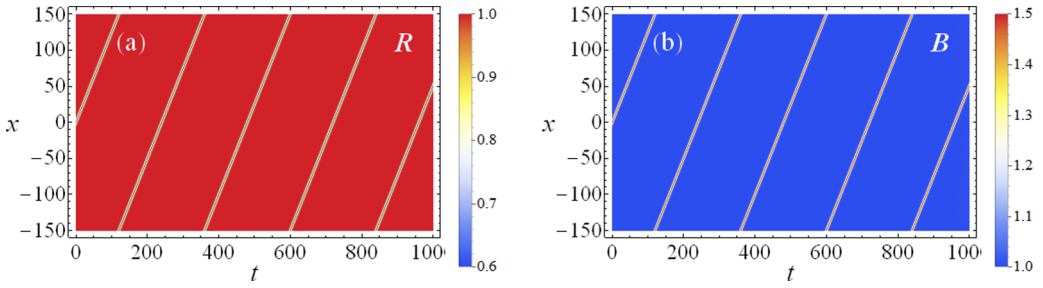


FIG. 2. Contour plots showing the spatiotemporal evolution of the solitary waves. Panel (a) [panel (b)] depicts the evolution of the $R$-component (the $B$-component) of the solution. Parameter values: velocity $v = 1.5$, $B_0 = R_0 = 1$ (i.e., $C = 1$), and $L = 150$.

and (33). Nevertheless, the system also possesses still another exact, but weakly localized, solitary-wave solution, which features an algebraic decay as the traveling-wave coordinate $\xi \to \pm\infty$. This solution exists in the limiting case in which $v = C$. Indeed, in this case, the ODE (26) reduces to the form

$$w'' = -\frac{3B_0}{2v^2}w^2 - \frac{1}{2v^2}w^3, \tag{46}$$

where now the fixed point $w = 0$ becomes an *inflection point* for the potential $V(w)$. In such a situation, it is possible to identify an exact, algebraically decaying, solution of Eq. (46), of the following form:

$$w(x,t) = -\frac{4B_0}{1 + R_0\xi^2}, \quad \xi = x - Ct. \tag{47}$$

This rational waveform gives rise to the following exact solution of the original AA model (7) and (8):

$$R(x,t) = R_0\left[1 - 4\frac{1 - n_0\xi^2}{(1 + R_0\xi^2)^2}\right] := R^r(x,t), \tag{48}$$

$$B(x,t) = B_0\left(1 - \frac{4}{1 + R_0\xi^2}\right) := B^r(x,t). \tag{49}$$

This solution, although interesting in its own right from a mathematical point of view, suggests an unphysical situation, namely a negative (inverse) density, as is clear from (49).

## III. NUMERICAL INVESTIGATIONS

In this section, we perform numerical simulations with an aim to investigate the dynamics of the solitary and periodic waves identified in the previous sections. First, we explore the dynamics of the single exact solitary wave when considered as an initial condition for the system. Second, we explore the dynamics of two solitary waveforms and their potential interaction dynamics. Third, we proceed to a numerical study examining the robustness of periodic solutions in the presence of Fourier mode perturbations. Finally, due to their mathematical interest (as they are not physically relevant in the context of the AA model), we briefly comment on the rational solutions.

The numerical integration is performed for the following initial-boundary-value problem of the AA system (7) and (8), with initial conditions

$$R(x,0) = \varrho_0(x), \quad R_t(x,0) = \varrho_1(x), \quad B(x,0) = \beta_0(x), \tag{50}$$

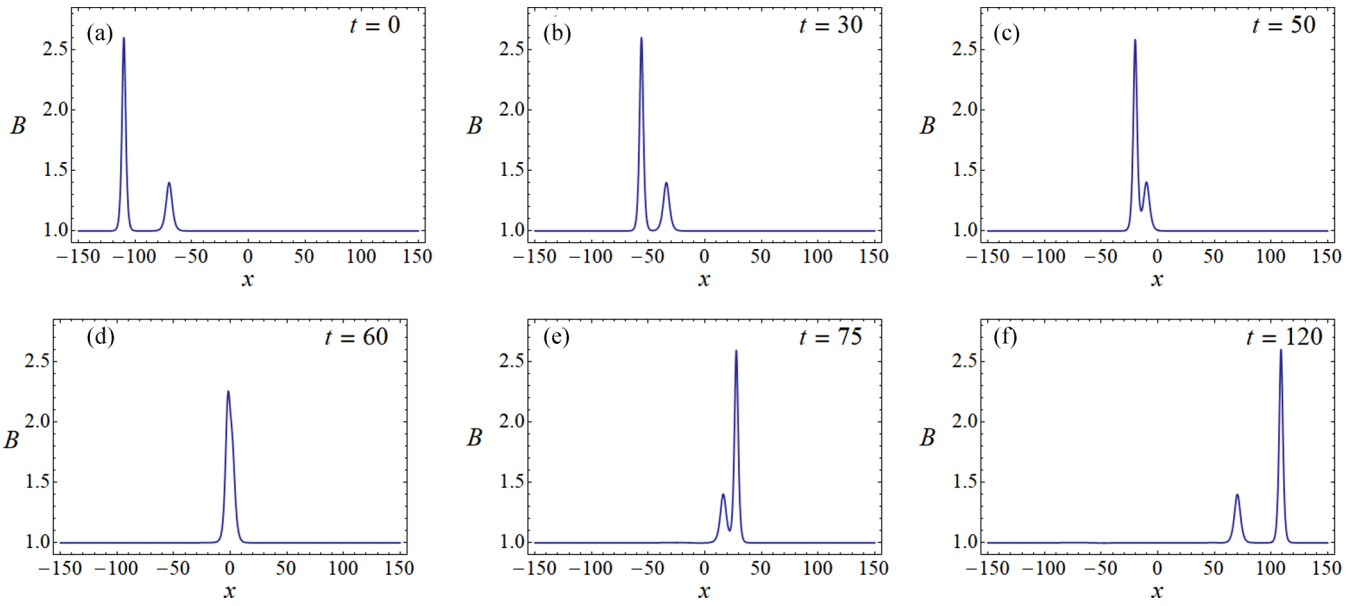


FIG. 3. Snapshots of the evolution of two colliding solitary waves. In each panel, the $B$-component of the solution is depicted. The initial positions and velocities for the solitary waves are $x_1 = -110$, $v_1 = 1.8$ and $x_2 = -70$, $v_2 = 1.2$. Parameter values are $B_0 = 1$, $R_0 = 1$, and $L = 150$.

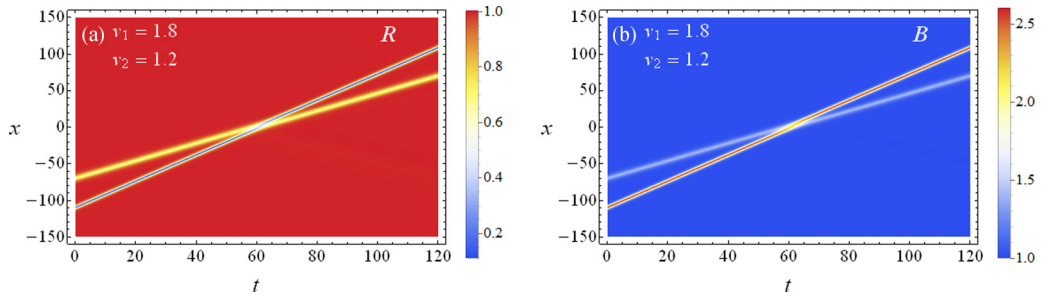


FIG. 4. Contour plots showing the spatiotemporal evolution of the two-soliton initial conditions $(R^{ds}(x,0), B^{ds}(x,0))$ for velocities $v_1 = 1.8$ and $v_2 = 1.2$. The rest of the parameters are fixed as in Fig. 3. Panel (a) [panel (b)] shows the $R$-component ($B$-component) of the solution.

and periodic boundary conditions on the interval $[-L, L]$, for $B$ and its first derivative $B_x$,

$$B(-L,t) = B(L,t), \quad B_x(-L,t) = B_x(L,t). \tag{51}$$

The initial-boundary-value problem [(7), (8), (50), and (51)] is integrated numerically by implementation of the method of lines [27]; a tensor product grid discretization scheme is considered for the spatial integration, while for the integration with respect to time a fourth- through fifth-order adaptive-step Runge-Kutta method is used.

### A. Dynamics of the single-soliton solutions

Numerical integration of the system (7), (8), (50), and (51) using as initial conditions the analytical solutions (32) and (33) at $t = 0$, i.e., $\varrho_0(x) = R^s(x,0)$, $\varrho_1(x) = R^s_t(x,0)$, $\beta_0(x) = B^s(x,0)$, verified the stability of their time propagation (and as a by-product, the accuracy of the numerical method). Their spatiotemporal evolution is depicted in the contour plots of Fig. 2. Panel (a) portrays the dynamics of the $R$-component of the numerical solution, while panel (b) portrays the dynamics of the $B$-component of the same solution. The system is integrated for $L = 150$, and for this choice the initial error at the boundaries is far smaller than the accuracy used in the calculations. The parameter values are $B_0 = 1$, $R_0 = 1$, $x_0 = 0$, while the velocity is $v = 1.5 > C = 1$, as $C$ is defined by (22). The initial data evolve as the exact soliton solutions (32) and (33), preserving their initial profile and speed.

### B. Interaction dynamics of two solitons

The second numerical experiment investigates the dynamics of two solitary waveforms, initialized by a superposition of the analytically derived soliton solutions presented in Sec. II B, i.e., (32) and (33). More precisely, we shall consider the dynamics of initial conditions of the form

$$R(x,0) = R_0 - \frac{1}{v_1^2} w_1(x,0)\left[B_0 + \frac{1}{2} w_1(x,0)\right] - \frac{1}{v_2^2} w_2(x,0)\left[B_0 + \frac{1}{2} w_2(x,0)\right] := R^{ds}(x,0), \tag{52}$$

$$B(x,0) = B_0 + w_1(x,0) + w_2(x,0) := B^{ds}(x,0), \tag{53}$$

with $w_i(x,t) = w(x,t)|_{(x_0 = x_i, v = v_i))}$, $i = 1, 2$, and $w(x,t)$ given by Eq. (29).

The expressions (52) and (53) describe the interaction between two solitons defined by the analytical solutions (32) and (33), with velocities $v_1$ and $v_2$, respectively. Here, it should be recalled that the permitted and physically relevant velocities should be such that $v_i \in (C, 2C] = (v_{\min}, v_{\max}]$.

We consider that the parameter values are $B_0 = 1$ and $R_0 = 1$, and thus $C = 1$. First, we examine the case in which the velocity of the first soliton $v_1 = 1.8$ is close to the upper boundary point $v_{\max} = 2$ of the permitted interval (1,2), and the velocity of the second soliton $v_2 = 1.2$ is close to the lower boundary point $v_{\min} = 1$. The system (7), (8), (50), and (51) is integrated for the initial conditions $\varrho_0(x) = R^{ds}(x,0)$, $\varrho_1(x) = R^{ds}_t(x,0)$, $\beta_0(x) = B^{ds}(x,0)$ for the above velocities $v_1$ and $v_2$. The first soliton is initially located at $x_1 = -110$ and the second soliton is at $x_2 = -70$. This choice ensures that the waves are well-separated, and at an adequate distance from the boundaries in order not to introduce any numerical arti-

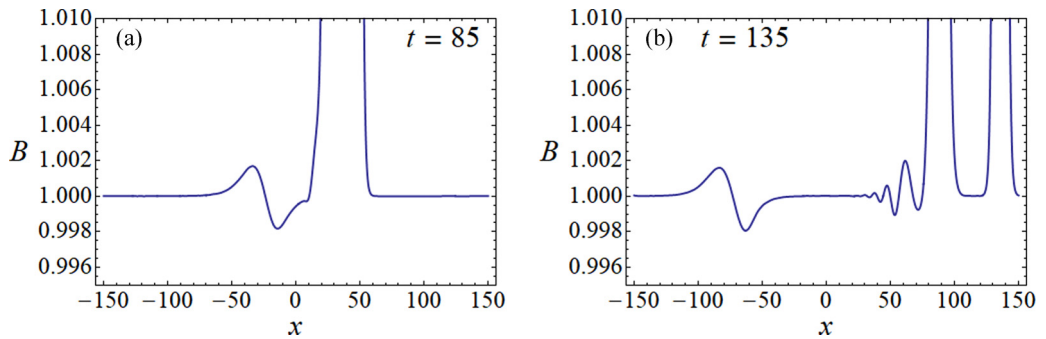


FIG. 5. Snapshots of the evolution of the two solitary waves with velocities $v_1 = 1.8$ and $v_2 = 1.2$. A magnification around the tail (during and after the collision of the solitons) of the $B$-component of the solution is shown. The rest of the parameters are fixed as in Fig. 3.

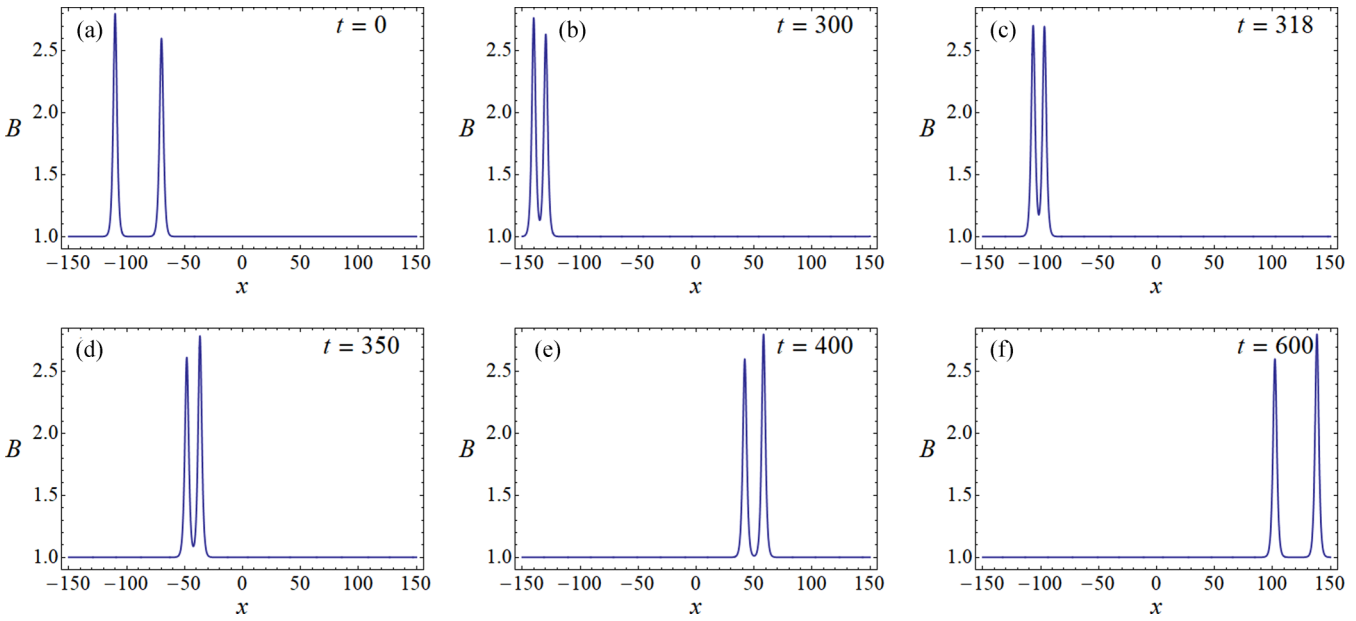


FIG. 6. Similar to Fig. 3, but now for solitons' initial positions and velocities $x_1 = -110$, $v_1 = 1.9$ and $x_2 = -70$, $v_2 = 1.8$. Parameter values are $B_0 = 1$, $R_0 = 1$, and $L = 150$.

facts. The system is integrated for $t \in [0, 200]$ and $L = 150$, which is a sufficient setting for the study of the interaction dynamics of the two solitons.

Figure 3 presents snapshots of the evolution of the $B$-component of the described two-wave initial condition (52) and (53) for $t \in [0, 120]$. The snapshots justify the collision of the two solitons and the near preservation (see the discussion below) of their initial profiles and velocities after their collision; the faster and taller soliton of velocity $v_1 = 1.8$ catches up with the slower and shorter soliton and eventually overtakes it.

The collision is alternatively visualized by the contour plots of the dynamics of the two-soliton initial conditions $R^{ds}(x, 0)$ and $B^{ds}(x, 0)$, depicted in Fig. 4. Panel (a) depicts the evolution of the $R$-component of the numerical solution, while panel (b) depicts the corresponding $B$-component.

An important finding is that the collision of the two solitons is nearly—but not genuinely—elastic. This fact suggests the nonintegrability of the system (7) and (8). This can be seen in Fig. 5, depicting snapshots of the dynamics of the $B$-component of the solution at $t = 85$ [panel (a)] and $t = 135$ [panel (b)], respectively, for the two solitary-wave initial conditions. The snapshots offer a magnified view around the tail of the solution, during and after the collision of the two waves. In both snapshots, we observe the emission of small-amplitude wave packets.

Next, we again fix $B_0 = 1$ and $R_0 = 1$, but now we will examine the dynamics of two waves initialized through $R^{\rm ds}(x, 0)$ and $B^{\rm ds}(x, 0)$, with velocities close to each other, but also being close to the upper boundary point $v_{\rm max} = 2$ of the permitted interval (1,2]. In particular, we use the values $v_1 = 1.9$ and $v_2 = 1.8$ and integrate the system for $t \in [0, 600]$ and $L = 150$. In this case, since the relative velocity of the two solitons is smaller, a larger time interval is required in order to study the corresponding interaction dynamics.

Figure 6 presents snapshots of the evolution of the two-wave initial condition $(R^{\rm ds}(x, 0), B^{\rm ds}(x, 0))$; each panel depicts the $B$-component of the solution. In this case, we observe an interaction of repulsive type: the two waves exchange their velocities, and afterward they continue their motion in the same direction. This interaction is also illustrated in the contour plots of Fig. 7; panels (a) and (b) show the dynamics of the $R$- and $B$-component of the solution, respectively.

In this case, the emission of small-amplitude waves is weaker if compared with that of the previous example for the velocities $v_1 = 1.8$ and $v_2 = 1.2$ (where we observed the collision). This is evident in Fig. 8, presenting snapshots of the evolution of the $B$-component of the solution, with a magnified view around its tail; the emerging wave packets are weak yet discernible in the snapshot for $t = 430$ [panel (c)]. Effectively, it can be observed here that the weak relative kinetic energy of the structures is not sufficient to overcome the potential energy barrier of the waves' repulsive interaction. As a result, a minimal dispersive wake is only emitted in the process.

### C. On the stability of the traveling solitary waves

Here, we comment on the stability of traveling solitary waves, relying on established stability criteria (see below). We start with the limit of $v \to C$, where the traveling solitary waves reduce to the KdV soliton [see Eq. (40)], as shown in the previous section. In this case, the relevant criterion, known for numerous decades [14–16], states the following: the KdV soliton is stable if $dN/dv > 0$, where $N[w] = \int_{-\infty}^{\infty} w^2 dx$ is a conserved quantity—namely the "momentum"—of the KdV equation. Figure 9(a) shows the dependence of $N[w]$ on the velocity $v$ for the KdV soliton of Eq. (45) [dashed (blue) curve]. In addition, shown also is the dependence of $N[w]$ on the velocity $v$ of the exact solitary-wave solution of Eq. (29) [solid (red) curve]; naturally, the latter curve approaches the former one (in line with our reduction) in the limit of $v \to C$.

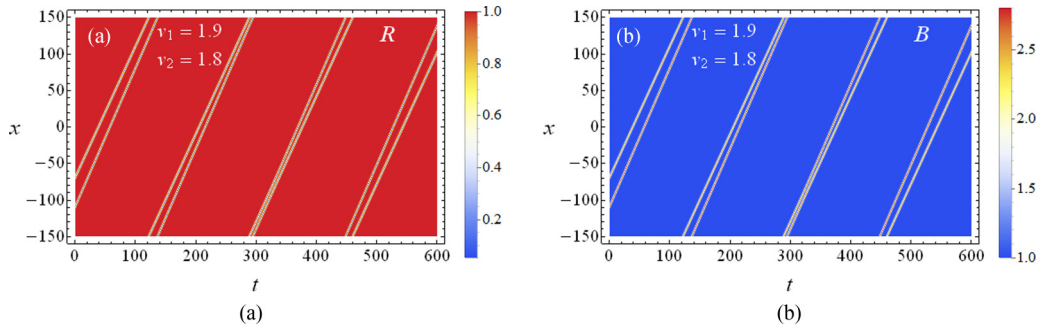


FIG. 7. Contour plots of the spatiotemporal evolution of the two solitary wave initial conditions $(R^{\rm ds}(x,0), B^{\rm ds}(x,0))$ for $v_1 = 1.9$ and $v_2 = 1.8$. The rest of the parameter values are fixed as in Fig. 6. (a) The $R$-component of the solution is shown. (b) The same as before but for the $B$-component.

It is readily seen that the KdV stability criterion is satisfied, definitively illustrating that our waves with speeds near the Alfvén speed are dynamically stable.

Another interesting aspect worth mentioning involves the recent work of [17] on quadratic operator pencils and associated stability criteria. Examining the condition of Eq. (4.8) therein in the case of a Klein-Gordon model, a short calculation shows that the relevant quantity controlling the stability amounts to the derivative of the Klein-Gordon momentum $P$ as defined by Eq. (18). Once again, the positivity of the relevant momentum derivative implies stability for the Klein-Gordon model, while the negativity thereof implies instability. Having derived the momentum of the AA system in Sec. II B [see Eq. (18)], and given its structural similarity with that of Klein-Gordon models, we have illustrated its dependence on the speed in Fig. 9(b). Here it is shown that $P$ is an increasing function of $v$ both in the KdV limit [dashed (blue) curve] and for the exact solitary-wave solution of the AA model [solid (red) curve]. Naturally, we appreciate that our model is neither of the KdV nor of the Klein-Gordon variety directly, hence while these criteria are suggestive (in that our model has a KdV limit and a Klein-Gordon type momentum), it remains an open question to rigorously illustrate the stability of traveling solitary waves of the present model. Nevertheless, all of the above observations, as well as our direct numerical computations for all relevant speeds, provide multiple pointers toward the generic stability of the Adlam-Allen traveling solitary waves and lead us to conjecture that this feature holds in the full range of (physical) solitary-wave velocities $(C < v < 2C)$.

### D. Periodic solutions

As was analyzed in Sec. II B, and visualized in Fig. 1, for energy values $E_0 < 0$, we detect spatially periodic, traveling-wave solutions, associated with the closed curves inside the homoclinic loop of the $(w, w')$ phase-plane. Let us recall that the bottom row of Fig. 1 shows the profiles of the $R^p(x,t)$-component [panel (a)] and of the $B^p(x,t)$-component [panel (b)] at $t = 0$ for such a spatially periodic solution (as denoted by the superscript $p$), corresponding to the energy $E_0 = -0.015$. We investigated numerically the stability of these spatially periodic solutions in the presence of small-amplitude, Fourier mode perturbations, considered as initial conditions of the dimensionless problem. Instead of the symmetric interval $[-L, L]$, the periodic boundary conditions (51) are implemented on the interval $[0, m\lambda]$, where $\lambda$ stands for the wavelength of the solution. The wavelength $\lambda$ can be calculated for a given set of parameters by integration of Eq. (28). In all of the examples considered herein, we assumed $B_0 = R_0 = 1$ and $v = 1.5$. The results are shown for $t \in [0, 200]$ for the sake of clarity of the presented graphics; however, we confirmed that the relevant solutions persist for at least twice the time horizon shown.

In Fig. 10, the spatiotemporal evolution of a perturbed spatially periodic initial condition is shown. The unperturbed initial condition $(R^p(x,0), B^p(x,0))$ explored is the one with energy $E_0 = -0.03$, where we have considered $m = 5$. In this condition, we perturb the $B$-component by adding a Fourier mode, and the initial condition becomes $(R^p(x,0), B^p(x,0) + 0.01\sin(3Kx))$, where $K = 2\pi/\lambda$ denotes the wave number associated with the wavelength $\lambda$ of the solution. More-

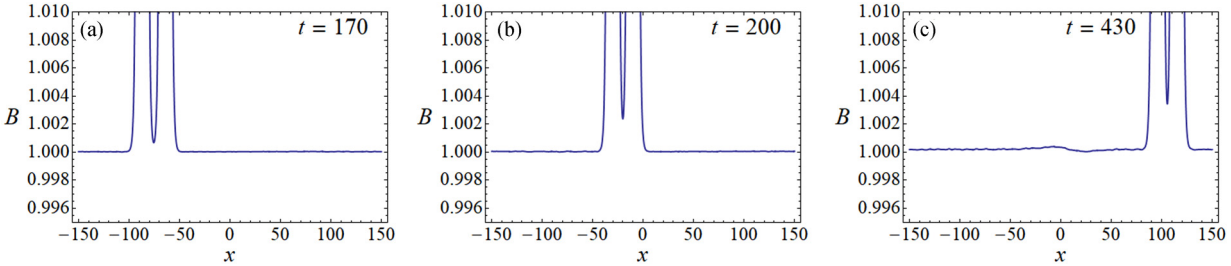


FIG. 8. Snapshots of the evolution of the two wave initial condition $(R^{\rm ds}(x,0), B^{\rm ds}(x,0))$, with velocities $v_1 = 1.9$ and $v_2 = 1.8$. A magnification around the tail, during the repulsive interaction of the solitons, of the $B$-component of the solution is shown. The rest of the parameter values are fixed as in Fig. 6.

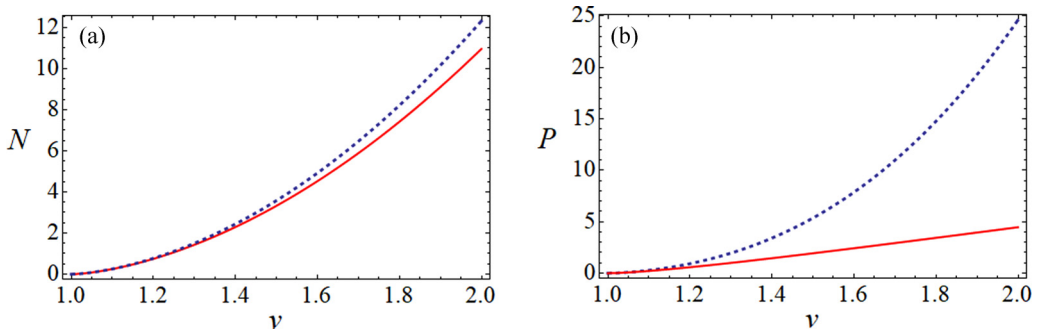


FIG. 9. (a) The dependence of $N$ on the velocity $v$. Here, $N(v)$ has been calculated in the small velocity (KdV) limit, using Eq. (45) [dashed (blue) curve], and for all permitted velocities, using Eqs. (13) and (14) [solid (red) curve]. It is observed that, in both cases, $dN/dv > 0$, which implies stability of the traveling solitary waves according to the KdV stability criterion (see the text). (b) The dependence of the momentum $P$ [Eq. (18)] on the velocity $v$. As in (a), the dashed (blue) curve and the solid (red) curve correspond to the KdV limit and the exact traveling wave [Eqs. (13) and (14)]. Observe that, in both cases, $dP/dv > 0$, which also suggests stability, per the discussion in the text.

over, Fig. 11 depicts the dynamics of another perturbed spatially periodic initial condition of the form $(R^p(x,0) + 0.01\sin(10Kx), B^p(x,0))$ for the example of $m = 3$. The unperturbed initial condition corresponds to energy $E_0 = -0.01$.

In both of the above examples, the evolution of the perturbed spatially periodic initial condition appears to robustly preserve the relevant waveform without giving rise to any growth modes, suggesting its dynamical stability. This is in line with what has been found in the case of cnoidal waves in the KdV equation; see, e.g., the work of [30].

### E. Rational solution

As was shown in Sec. II E, the case $v = C$ gives rise to a degenerate scenario for the dynamical system (46). Figure 12(a) shows the graph of the effective potential in this case: the potential $V$ has an inflection point at $w = 0$, and the energy $V(0) = E_0 = 0$ [continuous (green) horizontal line] defines the energy of a cusplike homoclinic connection in the $(w, w')$ phase plane; it is depicted by the continuous (green) curve in panel (b) (see also [31]). The corresponding analytical rational solutions $R^r(x,t)$ and $B^r(x,t)$ of the system are given by (48) and (49). The energy values $E_0 < 0$ [dashed horizontal curves in the panel (a)] are associated with the periodic orbits in the phase plane [dashed closed curves in panel (b)].

The spatial profiles of the coherent structure that is associated with the rational solution are illustrated in the bottom panels of Fig. 12. Panel (c) shows the $R^r(x,t)$ component at $t = 0$, and panel (d) shows the $B^r(x,t)$ component at $t = 0$.

We have attempted to integrate the system with initial conditions $R^r(x,0)$ and $B^r(x,0)$, but we have found that the dynamics is extremely sensitive to small perturbations giving rise to numerical instabilities. We have noted also that the kind of numerical instability appearing is dependent on the choice of the half-length $L$. This is to be expected given the algebraic decay-rate of the initial conditions. Thus, even for a choice of $L = 1000$ the initial error at the boundaries is of the order of $O(10^{-6})$, which can introduce numerical problems. In particular, considering these as small perturbations, the dynamical behavior of the solution turns out to be highly unstable.

This is a strong indication of the dynamical instability of this state. Thus, due also to its featuring negative density in part of the domain (hence being of rather limited physical relevance), we have not pursued it further.

## IV. CONCLUSIONS

We studied the Adlam-Allen (AA) system of partial differential equations, one of the prototypical and fundamental

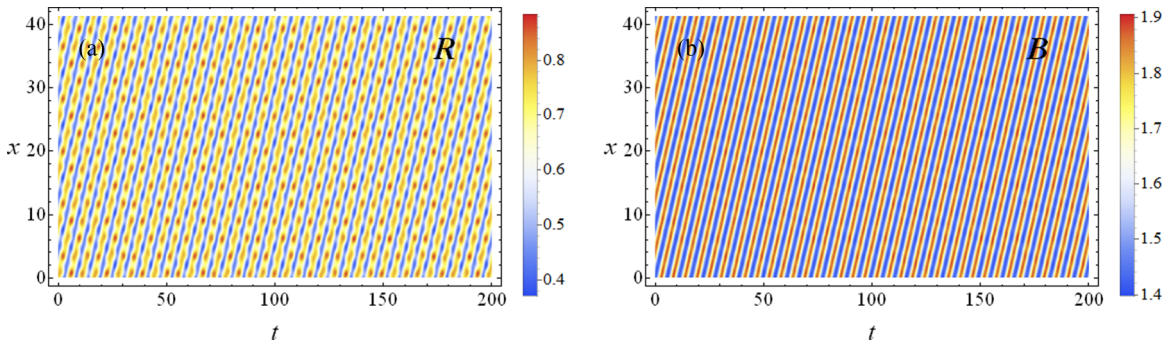


FIG. 10. Contour plot of the spatiotemporal evolution of the perturbed spatially periodic solution $(R^p(x,0), B^p(x,0) + 0.01\sin(3Kx))$. (a) The $R$-component of the solution. (b) The $B$-component of the solution. Parameter values: $B_0 = R_0 = 1$, $v = 1.5$. The spatial interval is $[0, m\lambda]$ with $m = 5$; $\lambda$ is the spatial period of the solution, and $K = 2\pi/\lambda$ is the wave number associated with the wavelength $\lambda$. The energy associated with the unperturbed initial conditions is $E_0 = -0.03$.

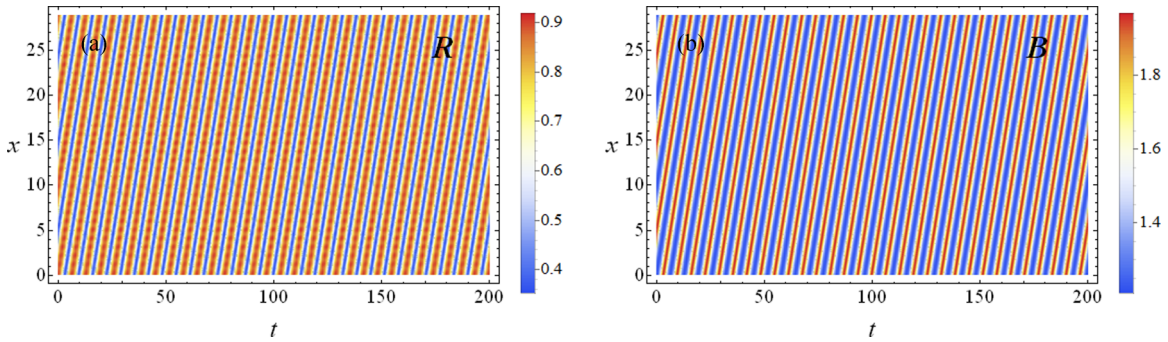


FIG. 11. Contour plot of the spatiotemporal evolution of the perturbed spatially periodic solution $(R^p(x,0) + 0.01\sin(10Kx), B^p(x,0))$ with $m = 3$. (a) The $R$-component of the solution. (b) The $B$-component of the solution. Parameter values: $B_0 = R_0 = 1$, $v = 1.5$. Energy of the unperturbed initial conditions $E_0 = -0.01$.

models for the description of hydrodynamic disturbances in collisionless plasmas. The phase-plane analysis for the relevant, effective second-order conservative dynamical system (associated with the description of traveling waves) enabled us to identify exact soliton solutions for the original system. In line with the original work of [1], we have found that these waves have velocities between one and two times that of the characteristic Alfvén speed.

Another important finding was that the Adlam-Allen system is strongly connected to the Korteweg–de Vries (KdV) equation: we have shown that, in the small-amplitude limit, the solitary waves of the original AA system transform into the soliton solutions of the Korteweg–de Vries equation. This connection was already highlighted when studying the linearization of the Adlam-Allen system: we found that this can be described by a linearized improved Boussinesq equation, which, in the long wave approximation and in the weak dispersion regime, features the same dispersion relation as the Korteweg–de Vries equation.

The above justifications motivated us to study by direct numerical simulations not only the dynamics of the exact soliton solutions but also the interaction dynamics of two soliton waveforms, initialized through a superposition of the analytical solitary waves. First, the stable evolution of individual exact pulses was observed in agreement with the analytical arguments for their derivation. In the more interesting case

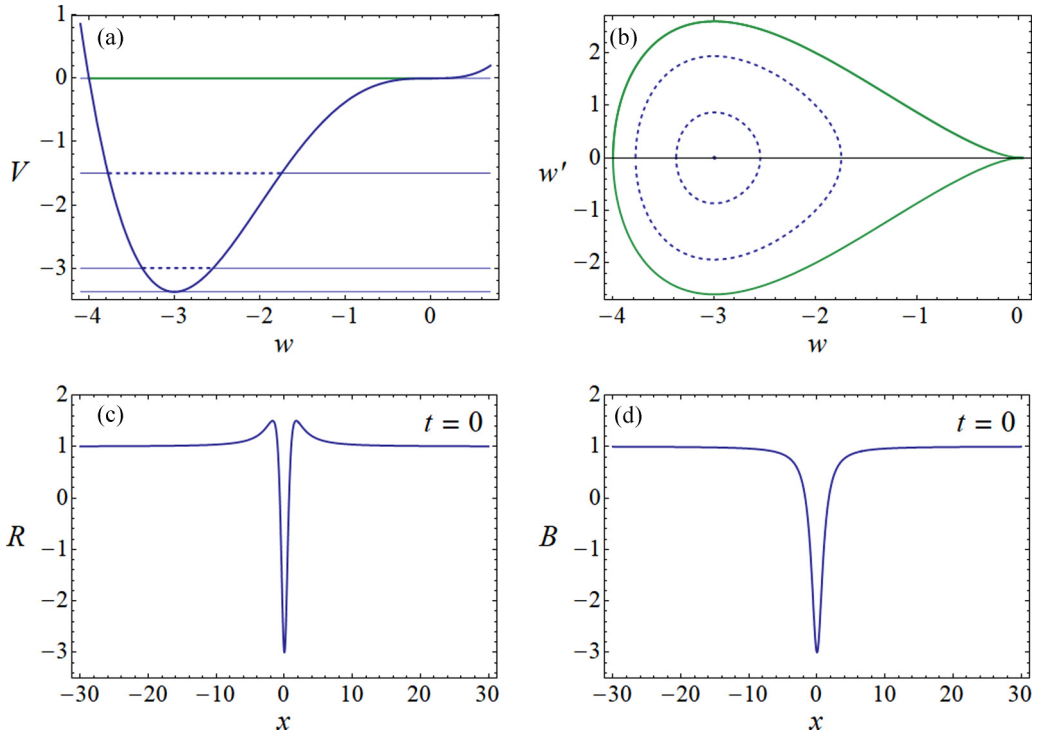


FIG. 12. (a) The graph of the effective potential when $v = C$, the case of the degenerate ODE, Eq. (46). The (green) horizontal line defines the energy $V(0) = E_0 = 0$ of the homoclinic connection associated with the analytical rational solutions (48) and (49). (b) The (green) continuous curve is the homoclinic connection of energy $V(0) = E_0 = 0$. The closed (dashed) periodic orbits correspond to energy values $E_0 < 0$ [dashed horizontal lines in (a)]. (c) The profile of the rational solution $R^r(x,t)$, given by Eq. (48), at $t = 0$. (d) The profile of the rational solution $B^r(x,t)$, given by Eq. (49), at $t = 0$.

of soliton interactions, we examined two scenarios. In the first scenario, in which the velocity of one soliton is close to the Alfvén speed and the velocity of the second is considerably higher, we found a quasielastic collision: the fast soliton overtakes the slow one, and both almost preserve their velocities and shape. The weak inelasticity of the collision was detected by the emission of small-amplitude linear waves. The occurrence of the latter is further suggestion that the Adlam-Allen system might be nonintegrable. In the second scenario, in which both soliton velocities take values close to twice the Alfvén speed, we observed an interaction of repulsive type; after an exchange of their velocities, the solitary waves continued their propagation in the same direction, emitting far weaker wave packets (in comparison to the previous case). Concerning the stability of the presented traveling solitary waves, we have brought to bear stability criteria both from the realm of KdV equations as well as from that of Klein-Gordon models. Pertinent results suggest that the solitary waves are stable (definitively so in the vicinity of the characteristic Alfvén speed), a conjecture that is also generically supported by our direct simulations that were performed in the full range of permitted velocities.

The dynamical systems analysis verified also the existence of spatially periodic solutions. A numerical study examining the dynamics of such solutions in the presence of small perturbations suggests that these spatially periodic traveling waves might be robust as well. Finally, the same dynamical analysis was used to reveal the existence of rational solutions, possessing an algebraic decaying rate in the limiting case of propagation at the Alfvén speed. It is worthwhile to note that such solutions are of growing interest due to their argued relevance within the context of rogue waves [28,29]. While such solutions are not of physical interest here (since they feature negative densities in part of the spatial domain), they are certainly of interest from a mathematical point of view. Remarkably, they are associated with a degenerate case of the effective conservative dynamical system. Yet, they are unfortunately found to be quite unstable numerically.

This study is only a first step toward an attempted revival of interest in the Adlam-Allen model. While we have explored special solutions and their full PDE dynamics, numerous questions remain. Among them, from a mathematical analysis point of view, well-posed properties (local and global) appear to us to be worthwhile to study, in analogy to the well-established counterpart of the KdV model. A more definitive view of the potential integrability of the problem (or, more likely, the lack thereof) could be an interesting direction to pursue in its own right. Finally, we note that this model concerns the analysis of a transverse magnetic field, while recently [32] the longitudinal, far more complex case has also been considered. Expanding the lines of thinking of the present work regarding multiple solitary waves and their interactions as well as generalized periodic solutions is also of interest. Work along these directions is currently in progress and will be reported in future studies.

## ACKNOWLEDGMENTS

This material is based upon work supported by the US National Science Foundation under Grant DMS-1809074 (P.G.K.). P.G.K. also acknowledges support from the Leverhulme Trust via a Visiting Fellowship and thanks the Mathematical Institute of the University of Oxford for its hospitality during this work.

[1] J. H. Adlam and J. E. Allen, Philos. Mag. **3**, 448 (1958).
[2] J. H. Adlam and J. E. Allen, Proc. Phys. Soc. **75**, 640 (1960).
[3] N. J. Zabusky and M. D. Kruskal, Phys. Rev. Lett. **15**, 240 (1965).
[4] E. Fermi, J. Pasta, and S. Ulam, Los Alamos report LA-1940 (1955), published later in Collected Papers of Enrico Fermi, E. Segré (Ed.), University of Chicago Press (1965).
[5] D. J. Korteweg and G. de Vries, Philos. Mag. **39**, 422 (1895).
[6] H. Washimi and T. Taniuti, Phys. Rev. Lett. **17**, 996 (1966).
[7] E. Infeld and G. Rowlands, *Nonlinear Waves, Solitons and Chaos* (Cambridge University Press, Cambridge, 1990).
[8] M. Kono and M. M. Skorić, *Nonlinear Physics of Plasmas* (Springer-Verlag, Heidelberg, 2010).
[9] J. E. Allen, Phys. Scr. **57**, 436 (1998).
[10] J. E. Allen and J. Gibson, Phys. Plasmas **24**, 042106 (2017).
[11] M. J. Ablowitz, *Nonlinear Dispersive Waves: Asymptotic Analysis and Solitons* (Cambridge University Press, Cambridge, 2011).
[12] N. G. Vakhitov and A. A. Kolokolov, Radiophys. Quantum Electron. **16**, 783 (1973).
[13] E. A. Kuznetsov, Phys. Lett. A **101**, 314 (1984).
[14] R. Pego and M. Weinstein, Philos. Trans. R. Soc. London A **340**, 47 (1992).
[15] D. E. Pelinovsky, in *Nonlinear Physical Systems: Spectral Analysis, Stability and Bifurcations*, edited by E. N. Kirillov and D. E. Pelinovsky (Wiley, Hoboken, NJ, 2014), p. 377.
[16] E. A. Kuznetsov, Phys. Lett. A **382**, 2049 (2018).
[17] J. Bronski, M. A. Johnson, and T. Kapitula, Commun. Math. Phys. **327**, 521 (2014).
[18] D. A. Tidman and N. A. Krall, *Shock Waves in Collisionless Plasmas* (Wiley Series in Plasma Physics, New York: Wiley-Interscience, 1971).
[19] K. Sauer, E. Dubinin, and J. F. McKenzie, Geophys. Res. Lett. **29**, 2226 (2002).
[20] C. M. C. Nairn, R. Bingham, and J. E. Allen, J. Plasma Phys. **71**, 631 (2005).
[21] N. Meyer-Vernet, *Basics of the Solar Wind* (Cambridge University Press, Cambridge, 2007).
[22] B. Malomed, D. Anderson, M. Lisak, M. L. Quiroga-Teixeiro, and L. Stenflo, Phys. Rev. E **55**, 962 (1997).
[23] A. Jeffrey and T. Kawahara, *Asymptotic Methods in Nonlinear Wave Theory* (Pitman Books Ltd, London, 1982).
[24] M. Remoissenet, *Waves Called Solitons* (Springer, Berlin, 1999).
[25] I. L. Bogolubsky, Comput. Phys. Commun. **13**, 149 (1977).
[26] I. S. Gradshteyn and I. M. Ryzhik, *Table of Integrals, Series, and Products* (Academic, Cambridge, 1994).

[27] W. E. Schiesser, *The Numerical Method of Lines* (Academic Press, San Diego, 1991).

[28] C. Kharif, E. Pelinovsky, and A. Slunyaev, *Rogue Waves in the Ocean* (Springer, New York, 2009).

[29] M. Onorato, S. Residori, and F. Baronio, *Rogue and Shock Waves in Nonlinear Dispersive Media* (Springer-Verlag, Heidelberg, 2016).

[30] N. Bottman and B. Deconinck, Discr. Cont. Dyn. Syst. A **25**, 1163 (2009).

[31] J. K. Hale and H. Koçak, *Dynamics and Bifurcations* (Springer-Verlag, New York, 1991)

[32] G. Abbas, J. E. Allen, M. Coppins, L. Simons, and L. James, Physics of Plasmas **27**, 042102 (2020).